Failure Analysis of Thick Composite Rings Under Diametral Compression

Hassan Mahfuz, Aloke Pal, Mojibur Rahman, and Shaik Jeelani
Tuskegee University's Center for Advanced Materials
Tuskegee, AL 36088
Leif Carlsson[*] and Peter Davies[**]
[*]*Mechanical Engg. Dept., Florida Atlantic University, Boca Raton, FL 33431*
****** *IFREMER Center de Brest, BP 70, 29280 Plouzane, France*

SUMMARY

Ring specimens extracted from thick composite cylinders with nominal thicknesses of 6 to 12 mm have been tested under diametral compression. Rings with three winding angles were tested to examine the effect of orientation on the structural integrity of the cylinder. The objective of this investigation was to determine the failure modes of ring specimens under the given compressive load. To enhance delamination, some of the specimens were fabricated with embedded teflon sheets to simulate delamination in the wall. Two sets of tests were conducted; one was with the implanted delamination and the other without the teflon inserts. Rings with teflon inserts were of particular interest to visualize the growth of delamination crack at various stages of loading. It was observed that ring failure occurred by an extension of the implanted delamination around the periphery of the ring. The cracks opened at the initial stage of loading but closed quickly as the load and delamination increased. The crack continued to grow almost symmetrically towards the top side of the ring, and final failure occurred due to massive fiber fracture at locations perpendicular to the loading axis. Finite element analysis using layered elements was performed to analyze the compressive testing of the ring specimens. Details of the experimental and finite element studies are presented in this paper.

KEYWORDS : composite structures, blucking, finite element method (FEM)

INTRODUCTION:

Cylindrical pressure vessels are widely used in commercial as well as in defense applications. The emergence of composite materials with high specific strength and stiffnesses, has tempted both the commercial and defense sectors to consider these composites in the manufacturing of cylinders. The application of these cylinders ranges from aerospace, to navy, and to transportation industries [1-3]. The primary objectives are to obtain substantial saving in weight and significant improvement in strength. Of particular interest in this study is the investigation of thick composite cylinder under external pressure.

For thick-walled pressure vessel the state of stress or strain is three dimensional, and delamination is most likely a potential failure criterion. To study the delamination growth in cylinder wall, a simplified approach is taken in this investigation. Ring specimens extracted from thick-walled cylinders have been subjected to compressive load along the diameter. Ring tests of this type are particularly attractive to users of

cylindrical structures, as they can be used for quality control purposes and to simulate the response of a structure [4-5].

Analytical formulations to calculate stresses in rings under diametral compression goes back to the earlier part of this century [6-8]. While closed form solutions can be obtained for isotropic materials, it will be formidable to come up with such solution in case of composite rings. The degree of difficulty will further increase if the rings are intentionally delaminated at discrete locations in the wall. One is therefore, left with the option of using finite element method to assess the distributions of stresses and strains.

In the present paper a comprehensive study has been carried out to investigate the delamination growth in ring specimens under diametral compression. Rings with and without implanted delamination have been tested using a fixture especially developed for this purpose. ANSYS [9] finite element code has been used to develop models with implanted delamination, and interlaminar stresses have been computed for failure analysis.

EXPERIMENTS:

Composite cylinders were fabricated using filament winding. E-glass fibers in an epoxy resin were used in the manufacture of the cylinders. The epoxy system used in the fabrication was LY556/HY917 and the reinforcing fibers were 2400 tex E-glass manufactured by Vetrotex. Cylinders were fabricated with two wall thicknesses; 6 and 12 mm. Three sets of winding angles; $\pm 30^0$, $\pm 55^0$, and $\pm 85^0$, were considered during fabrication. It is to be noted that the winding angles indicated here are the angles with the longitudinal axis of the cylinder. The average inner diameter of the cylinders was approximately 159.5 mm. Ring specimens of width 20 mm were cut from the cylinders for the diametral compression tests. The cylinders were of two categories; one set was manufactured with 25.4 μm thick teflon inserts at the mid-thickness of the cylinder to define a delamination, while the second set contained no inserts.

A test fixture as shown in Fig. 1 was developed to test the specimens under diametral compression. The test fixture is consisted of two thick plates, one each at the top and bottom of the ring. To keep ring specimens properly aligned and upright, two vertical guide plates were welded to the two base plates. The gap between the two guide plates are such that they can accommodate various sizes of ring specimens. There are number of threaded holes on the guide plates through which set screws can be used to position the ring between the guide plates. To prevent any accidental slippage of the specimen during the test, two protector plates were provided on both left and right hand side of the specimen. The height and location of the protector plates were designed carefully to contain the specimen securely during any slippage, and at the same time without restricting the actuator movement and expansion of the ring during the test. During the test, the teflon-inserted side of the ring was always with the bottom platen, which in turn was attached to the actuator of the MTS machine.

A total of 37 ring specimens were tested using the fixture mentioned above. Out of these 37 specimens, 14 specimens were with teflon inserts and the rest were virgin. The tests were conducted in an MTS machine under displacement control mode with a constant displacement of 1.27 mm/min. Strain gages were bonded to the inner wall of each specimen at 0^0 and 90^0 locations as shown in Fig. 2. Both strain gages were placed

in the hoop direction. Strain gages were connected to strain indicators so that strain values could be monitored at various stages of the loading.

One of the objectives of this study was to monitor the growth of delamination at the location of the teflon inserts. To observe the in-situ progress of crack propagation, a tele-microscope was employed during the test. A dial indicator as shown in Fig. 2 was attached to the inner wall of the ring to monitor the crack opening during the test. The load vs. cross-head displacement was monitored from the MTS data recorder. The difference between the actuator displacement and the dial gage reading was taken as the opening displacement for the crack.

FINITE ELEMENT MODELS:

Three sets of finite element models corresponding to three winding angles were developed using the commercial finite element code; ANSYS [9]. Eight noded isoparametric layered solid elements (SOLID46) were used to develop the FEM models. This is a layered version of the 8-noded structural solid element which allows up to 100 different material layers, and has three degrees of freedom at each node; translations in the nodal x, y and z directions. Material properties used in the FEM analysis were; E_1=40 GPa, E_2=10 GPa, G_{12}=4.5 GPa, G_{23}=4.0 GPa, $\nu_{12} = \nu_{23} = 0.3$. These properties were taken from the reference [4]. Only the 12 mm thick rings were analyzed using the finite element studies. A gap of length 25 mm, and of opening .0254 mm as shown in Fig. 2, was created in the model to simulate the implanted delamination. The crack tip was modeled by collapsing the 8-noded element into a triangular form. A total of 24 layers were considered along the thickness. To obtain the distribution of stresses along the wall, the thickness of the ring was modeled with 4 elements each containing 6 layers. The entire model was generated with 648 elements consisting of 3888 nodes. The load was applied along a line at five nodes on the bottom surface of the ring. The displacements of these five nodes were constrained in all directions except in the direction of the loading. Multiple loading steps were used to account for the geometric non-linearity. The magnitude of the load was equal to the measured failure load in each case. The displacements of the nodes on the diametrically opposite side of the ring were constrained completely to simulate the rigid support.

RESULTS AND DISCUSSION:

Experimental Studies

Load-deflection curves for the 12 mm thick specimens with $\pm 85^0$ orientation with and without delamination are shown in Fig. 3. Figure 3 shows that the load-deflection behavior of both rings are similar. There is slight reduction in failure load in case of specimen with delamination as seen in Fig. 3. At other orientations, the reduction in failure loads were however, different. Percentage reduction in failure loads at various winding angles due to the presence of delaminations are shown in Table1. It is observed that the wall-thickness has a direct bearing on the growth of delamination. In general, the percentage reduction is more with higher wall-thickness, suggesting that interlaminar stresses become more prominent as the thickness increases.

As mentioned earlier, rings with three winding angles were tested to determine the effect of orientation on the compressive failure load. Table1 depicts the variation of failure load as a function of winding angle. It is observed that winding angle has a

profound influence on the failure of the ring specimens. As the winding angle increases, the failure load increases. This is true for specimens with and without delamination, and also for both the thicknesses. The failure load increased from 2.5 to 5 times as the angle increased from $\pm 30^0$ to $\pm 85^0$. Higher failure loads at $\pm 55^0$ and $\pm 85^0$ orientations suggest that as the fiber alignments tend more towards becoming perpendicular to the axis, the ring specimens become more and more stable under diametral compressive loading. From physical point of view this can be visualized as that at $\pm 85^0$ winding angle, the fibers are almost aligned in the hoop direction of the ring which allows the ring to sustain higher hoop stress prior to failure.

The effect of thickness on the compressive strength is shown in Fig. 4. This figure shows the load-displacement curves of $\pm 85^0$ rings for two thicknesses. An increase in thickness by 100% as seen in Fig. 4, increases the strength by almost three fold. Lower slope of the load-displacement curve for the 6mm thick specimen as observed in Fig. 4 is quite understandable. The thinner the wall, the lower will be the resistance of the ring to the external load. Load deflection curves for other winding angles have also been investigated. Load-deflection behavior for three winding angles are shown in Fig. 5. It is found that rings with $\pm 30^0$ orientation undergo permanent deformation before failure. However, that is not the case with $\pm 55^0$ and $\pm 85^0$ rings. It is noticed that diametral displacements at failure loads are also proportional to the winding angle. As winding angle increases, the failure displacement increases. This again indicates that $\pm 85^0$ angle is the most preferred orientation under diametral loading situation.

It was of particular interest in this investigation to monitor the growth of delamination due to the presence of teflon inserts. In-situ monitoring of delamination growth during the testing of the ring indicates that delamination initiates at the tips of the implanted delamination at an early stage of the loading, and extends symmetrically towards the 90^0 locations of the ring. With the increase in load, delamination continues to grow along the periphery until the ring fails by tensile failure of the fibers at 90^0 locations. In order to show the growth of delamination from 0^0 towards 90^0 location and beyond, SEM studies were performed on post-fractured specimens. The SEM specimens were cut from the fractured ring specimens at various locations. One such SEM micrograph is shown in Fig.6 for $\pm 85^0$ ring. The figure shows significant delamination at 90^0 location along the hoop direction.

One other observation near the teflon area was that the opening and closing of the crack took place only between 2-5.33 KN load range. The crack opened at around 2 KN, continued to open until 3.6 KN, and then began to close as the load increased. The crack completely closed around 5.3 KN load, and it remained closed through the remainder of the loading. This phenomenon was concentrated only at the location of the teflon, however, the delamination growth continued along the periphery as stated earlier. The crack opening displacements with respect to load is shown in Fig. 7

FEM Analysis:

To analyze the failure modes of the ring specimen, distributions of hoop, radial and interlaminar shear stresses were considered at various locations of the ring. Three locations, namely, AB, EF and CD as shown in Fig. 2 were of particular interest since most of the failures either initiated or occurred at those locations. All three sections are

along the thickness of the wall. Section AB is along the loading axis and on the loading side of the ring (that is bottom side), EF is at the location of the implanted crack-tip about 2.5^0 away from the loading axis (0^0), and CD is 90^0 away from the loading axis. Through-thickness distributions of hoop and radial stresses are shown in Figs 8 and 9. Hoop stress magnitude across EF is negligible, and its effect will be minimal in causing any damage to the laminate near the crack tip. It is however, interesting to note that the hoop stress magnitude near the crack tip increases by a large factor from what are found near the edges. This is surely due to the presence of the crack. If one moves to 10^0 for example (not shown in Fig. 8), that is 10^0 away from the tip, the hoop stress distribution almost reverses. It is higher at the edges and minimum near the mid-thickness. Along CD, hoop stress distributions are as expected. High stress magnitudes shown at C and D are most likely to cause laminate failure both at the inner and outer periphery of the ring in the form of matrix crack and fiber rupture.

In case of radial stress distribution, the scenario is somewhat different. It varies approximately from +1300 MPa to -1300 MPa both along AB and EF as shown in Fig. 9. The stresses are large at the edges and they change sign at the mid-thickness location. This reversal of stresses takes place in the region of the crack and also at locations away from the crack. FEM results (not shown here) indicate similar trend at 10^0, 20^0 and 30^0 locations. The presence of the crack does not reverse the trend of stress distribution as it did in case of hoop stress. It is also to be noted here that, +1300 MPa radial stress at the inner radius means compressive stress at A, while -1300 MPa at the outer wall also means compressive stress at B, since σ_r is taken as positive towards increasing r. It is therefore, obvious that reversal of σ_r will cause interlaminar tension at the mid-thickness location. We believe this is one of the reasons that delamination in the ring takes place at mid-thickness region regardless of the presence of the crack, and it continues beyond the location of the crack.

FEM model predicts large concentration of interlaminar shear stress at the crack tip as shown in Fig. 10. If we define a stress intensity factor as a ratio of the tip-stress to the edge-stress, a factor as high as 2 can be found. This ratio however, changes with the winding angle as seen in Fig. 10. The higher the winding angle, the higher is the ratio. The magnitude of the stress also increases consistently with the winding angle. At locations other than the region of the implanted crack, the magnitude of the stress is almost negligible. The stress distributions examined at 10^0 , 20^0 and 30^0 (not shown here) locations indicate that there is no spike at the mid-thickness area as observed in Fig. 10. The stress concentration shown in Fig. 10 is therefore due to the presence of the crack. What we now observe from Figs. 9 and 10 that both interlaminar shear and interlaminar tensile stresses generated in the region of the crack, are sufficient to sustain a continuous growth of delamination along the periphery.

A comparison of the load-displacement response as obtained from the experiment and FEM are shown in Fig. 11. Since the material properties are constant during the iteration, the FEM curve is linear throughout the loading range. The slopes of the load-displacement curves indicate that FEM cannot capture the experimental response during the initial loading period. However, as the load increases, the difference between the two reduces, and the correlation is reasonable. It is also noted in Fig.11 that the knee in the experimental curve is corresponding to 4.45 KN, which is close to 5.33 KN value

indicated earlier in Fig. 7. The crack begins to close in this loading range. It is therefore, observed that FEM results correlate better after the closure of the initial crack.

SUMMARY:

The following conclusions are drawn from the current investigation:

- The strength of the ring specimen under diametral compression is a direct function of the winding angle. The higher the winding angle, the higher is the failure load.
- Wall thickness of the ring has a direct bearing on the growth of delamination. Percentage reduction in strength due to the presence of implanted delamination increased with increased wall thickness.
- The crack opening pattern in the ring is quite different from what is usually observed in a Double Cantilever Beam (DCB) test. The crack opens up to a certain portion of the initial loading, it begins to close as the load increases, and then remains closed through the remainder of the loading until final failure takes place.
- Delamination in the ring however, continues to grow along the periphery beginning from initial loading to final failure regardless of the opening or closure of the implanted crack.
- Final failure of the ring takes place at locations perpendicular to the loading axis due to tensile fracture of fibers at the outer wall or compressive failure of matrix at the inner wall. Major failure modes are identified as; delamination along the periphery at mid-thickness area, and fiber fracture accompanied by matrix cracks at 90^0 location.
- Finite element analysis predicts that there will be sufficient concentration of hoop and interlaminar stresses that will allow the continuation of the crack growth beyond the implanted delamination zone. FEM analysis further shows that there is a reversal of radial stress sign in the mid-thickness region of the wall which will generate sufficient interlaminar tensile stresses to support a continuous growth of delamination in that region.

REFERENCES:

1. Tsai, S.W., *Composites Design*, 4th edition, Think Composites, Dayton, Ohio.
2. Bert, C.W., "Analysis of Radial Filament-Reinforced Spherical Shells Under Deep Submergence Condition, 2nd Intl. Conference on Pressure Vessel Technology, Part-I, design and Analysis, ASME Oct. 1973, pp. 529-534.
3. Beckwith, S.W., et. Al., "Filament wound Case (FWC) Graphite/Epoxy Pressure Vessel Response to Environmental Conditioning", 21 Intl. SAMPE Symposium, April 7-10, 1986, Las Vegas.
4. Pierron, F. and Davies, P., "Ring Compression Test for Cylindrical Composite Mechanical Characterization," Presented at the ECCM-CTS4 conference, August 31, 1998, Lisbon.
5. Peters, S.T. and Humphrey, W.D., *ASM Engineered Materials Handbook on Composites*, 1987.
6. Timoshenko, S.P. and Goodier, J.N., *Theory of Elasticity*, 3rd Edition, McGraw-Hill Book Company, New York.
7. Filon, L.N.G., "The Stresses in A Circular Ring," Selected Engineering Papers, No. 12, London, 1924, Published by the Institute of Civil Engineers.

8. Ripperger, E.A. and Davids, N., “Stress Evaluations in Circular Rings,” Trans. ASCE, Vol. 112, pp. 619-628, 1947.
9. *ANSYS Engineering Analysis System*, Swanson Analysis Systems Inc., Houston, Pennsylvania.

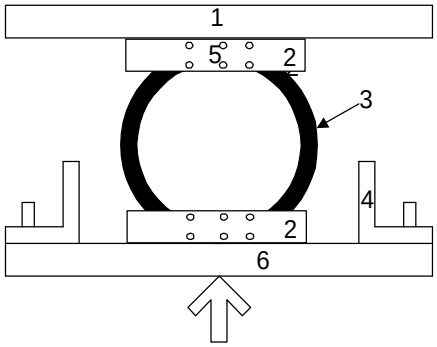

1. Top Plate 4. Protective Plate
2. Guide Plate 5.Threaded Holes for set Screws
3. Ring Specimen 2.Bottom plate

Fig.1: Test Fixture for Diametral Compression Tests

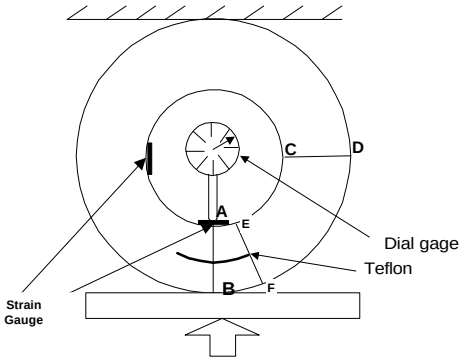

Fig.2: Location of Teflon Inserts and Strain gages

Thickness	Winding Angle	Failure Load (N)		Percentage Reduction in Failure Load
		Without Teflon	With Teflon	
12 mm	$\pm 85^0$	12638	11276	10.8
	$\pm 55^0$	11765	5519	53.0
	$\pm 30^0$	4851	2983	38.5
6 mm	$\pm 85^0$	4708	4107	12.7
	$\pm 55^0$	1714	1514	11.6
	$\pm 30^0$	717	660	8

Table1: Percentage Reduction in Failure Load due to the Presence of Teflon Inserts

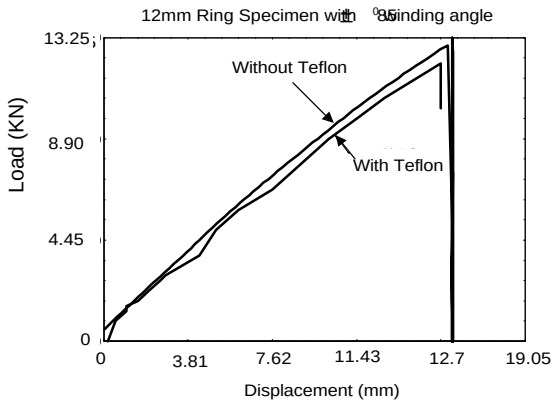

Fig. 3: Load-Displacement Behavior

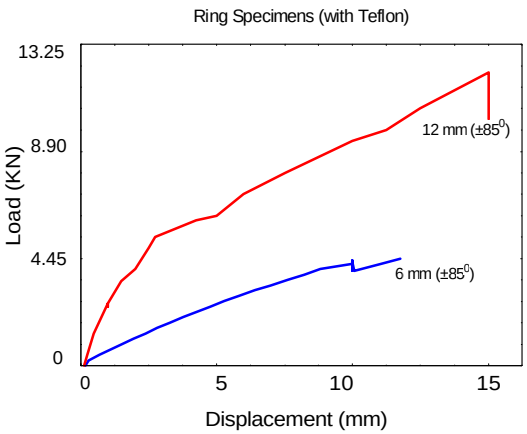

Fig.4: Effect of Thickness on Load-Displacement Behavior

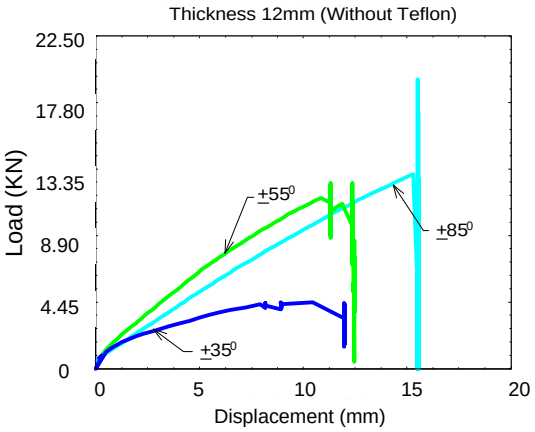

Fig.5: Load-Displacement Curves for Three Winding Angles

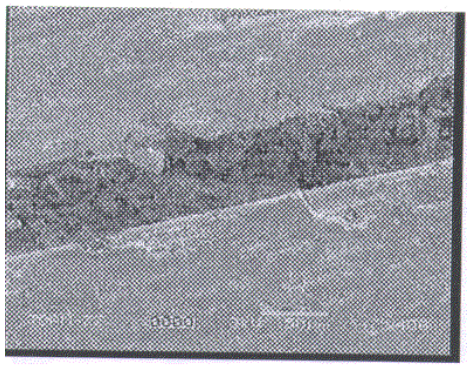

Fig. 6: Delamination at 90^0 Location

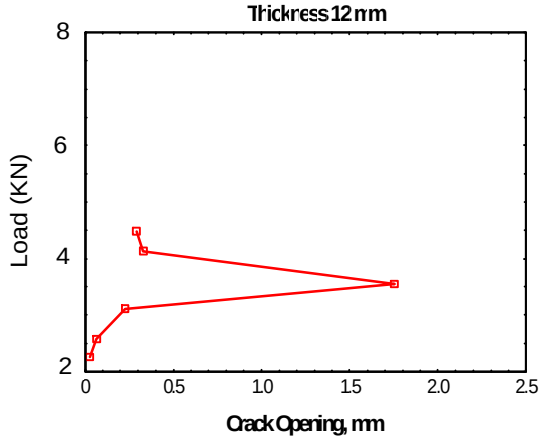

Fig. 7: Crack Opening Displacement a as Function of Applied Load

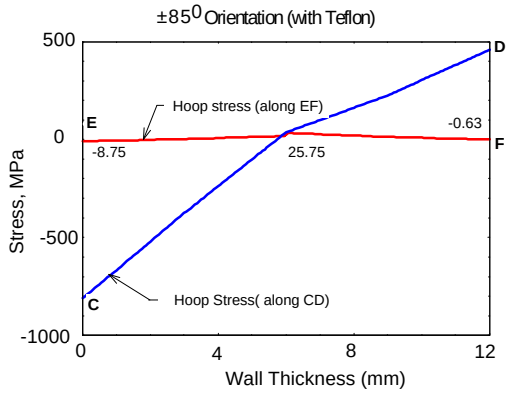

Fig. 8: Hoop Stress along Wall Thickness

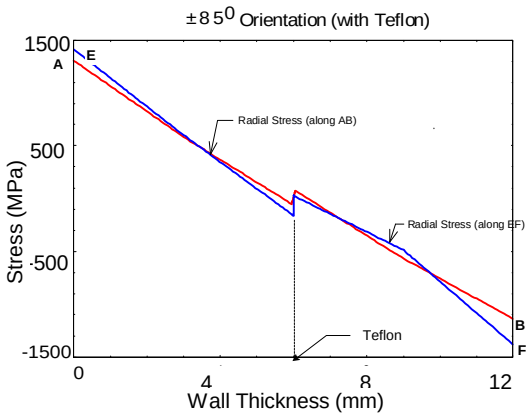

Fig.9: Radial Stress along Wall Thickness

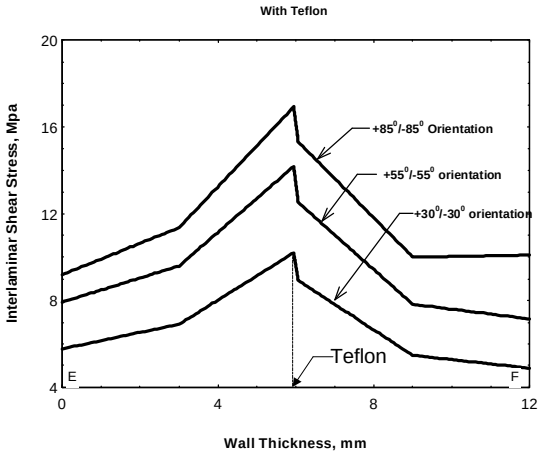

Fig. 10:Interlaminar Shear Stress Distributions for Various Winding Angles

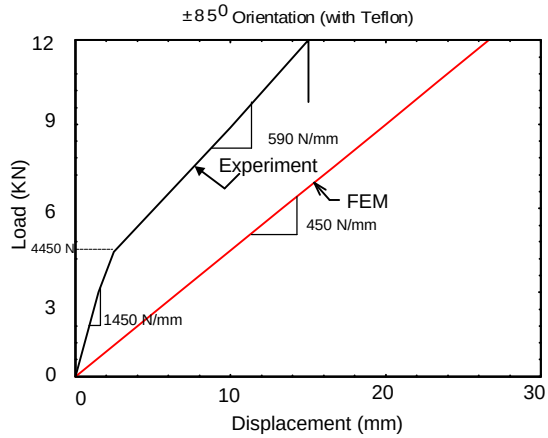

Fig. 11: Comparison of Load-Deflection Response